Available online at www.sciencedirect.com
SCIENCE DIRECT®
Chaos, Solitons and Fractals 22 (2004) 1165–1182
CHAOS SOLITONS & FRACTALS
www.elsevier.com/locate/chaos

Chaos anticontrol and synchronization of three time scales brushless DC motor system

Zheng-Ming Ge *, Jui-Wen Cheng, Yen-Sheng Chen

Department of Mechanical Engineering, National Chiao Tung University, 1001 Ta Hsueh Road, Hsinchu 300, Taiwan, ROC

Accepted 18 March 2004

Abstract

Chaos anticontrol of three time scale brushless dc motors and chaos synchronization of different order systems are studied. Nondimensional dynamic equations of three time scale brushless DC motor system are presented. Using numerical results, such as phase diagram, bifurcation diagram, and Lyapunov exponent, periodic and chaotic motions can be observed. By adding constant term, periodic square wave, the periodic triangle wave, the periodic sawtooth wave, and $kx|x|$ term, to achieve anticontrol of chaotic or periodic systems, it is found that more chaotic phenomena of the system can be observed. Then, by coupled terms and linearization of error dynamics, we obtain the partial synchronization of two different order systems, i.e. brushless DC motor system and rate gyroscope system.

1. Introduction

Chaotic phenomena are observed widely in many physical systems. It is interesting because of its apparent randomness and unpredictable behavior which is due to sensitive dependency on initial conditions.

Anticontrol is an interesting, new and challenging phenomenon [6–22]. It has a great potential for application to biological systems for future applications, such as control of heart beating and neuronal system [1].

Chaos synchronization has been studied extensively during the past two decades [2,3,24–37]. Traditionally, synchronization has been limited to periodic signals only. Now, chaotic signals can also be used for synchronization of either identical or different chaotic systems. Chaos synchronization has potential applications in such as chaos control, information processing, and secure communication.

In this paper, we will present the blushless dc motor system (BLDCM), which is transformed to a nondimensionalized form at the beginning. Then we study the behavior of BLDCM via adding various terms. By applying the numerical results such as phase portrait, and bifurcation diagram, a variety of the phenomena of the chaotic motion can be presented. Furthermore, chaotic motion can be checked by Lyapunov exponents. Anticontrol of chaos is studied via a constant torque, a $x|x|$ term, and a periodic wave, i.e. the square wave, the triangle wave, or the sawtooth wave. Then, we study the synchronized behavior of two different order systems, i.e. the BLDCM system and rate gyroscope system by various coupling terms, and linearization of error dynamics. Finally, the conclusions of the whole paper are briefly stated.

* Corresponding author. Tel.: +886-35712121; fax: +886-35720634.
E-mail address: zmg@cc.nctu.edu.tw (Z.-M. Ge).

0960-0779/$ - see front matter © 2004 Elsevier Ltd. All rights reserved.
doi:10.1016/j.chaos.2004.03.036

2. Description of the three time scales brushless DC motor differential equations of motion

2.1. Description of brushless DC motor system and its differential equation of motion

The system considered here is shown in Fig. 1. The brushless DC motor (BLDCM) is an electromechanical system. Its dynamic equations of electrical part can be described by [4,5]

$$\frac{\mathrm{d}}{\mathrm{d}t}i_q = \frac{1}{L_q}[-Ri_q - n\omega(L_d i_d - k_t) + v_q] \tag{2.1}$$

$$\frac{\mathrm{d}}{\mathrm{d}t}i_d = \frac{1}{L_d}[-Ri_d + nL_q\omega i_q + v_d] \tag{2.2}$$

and the dynamic equation of mechanical part is

$$\frac{\mathrm{d}}{\mathrm{d}t}\omega = \frac{1}{J}[T(I,\theta) - T_\ell(t)] \tag{2.3}$$

where

L_d, L_q: the fictitious inductance on the direct-axis and quadrature-axis,
v_d, v_q: the direct-axis and quadrature-axis voltage,
i_d, i_q: the direct-axis and quadrature-axis current,
n: number of permanent pole pairs,
ω: the rotor angular speed,
R: winding resistance,
J: the inertia momentum,
$k_t = \sqrt{\frac{3}{2}}k_e$: k_e is the permanent-magnet flux constant,
θ: the displacement variable,
$I = [i_q i_d]^{\mathrm{T}}$.

$T_\ell(t)$ is the external torque caused by cogging and friction imposed on the shaft of the motor. If viscous damping is considered, then the external torque

$$T_\ell = b\omega + T_L$$

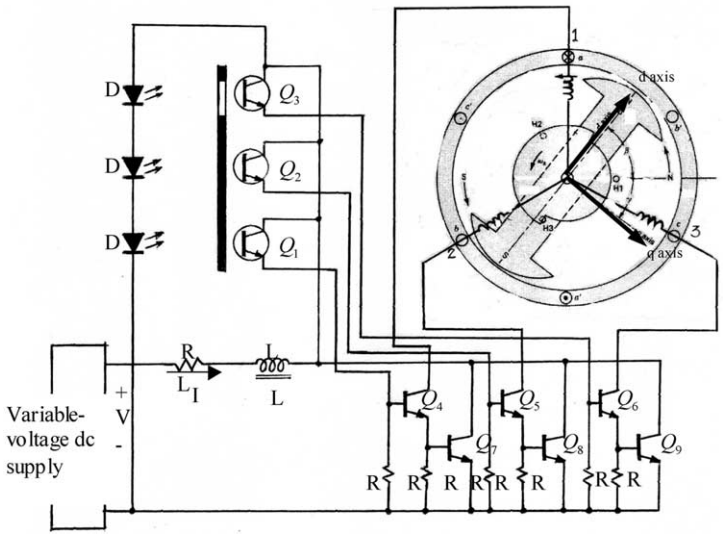

Fig. 1. Typical brushless dc motor and its commutation.

where b is the viscous damping coefficient, T_L the additional terms such as external load, cogging effects, coulomb friction, etc. and θ is eliminated by transforming the motor dynamics to the rotating frame, the electromagnetic torque $T(I,\theta)$ is given by

$$T(i_q, i_d) = n[k_t i_q + (L_d - L_q) i_q i_d]$$

So we can get

$$\frac{\mathrm{d}}{\mathrm{d}t}\omega = \frac{1}{J}[n[k_t i_q + (L_d - L_q) i_q i_d] + \frac{1}{J}(b\omega + T_L) \tag{2.4}$$

2.2. Three time scales representation of equations of motion and the computational analysis

In this section, Eqs. (2.1), (2.2) and (2.4) will be transformed to another statespace model and it can reduce the number of system parameters [4]. The multiple time scales are τ_1, τ_2, and τ_3, where

$\tau_1 = \frac{L_q}{R}$: the first electrical time constant

$\tau_2 = \frac{L_d}{R}$: the second electrical time constant

$\tau_3 = \frac{JR}{k_t^2}$: the mechanical time constant

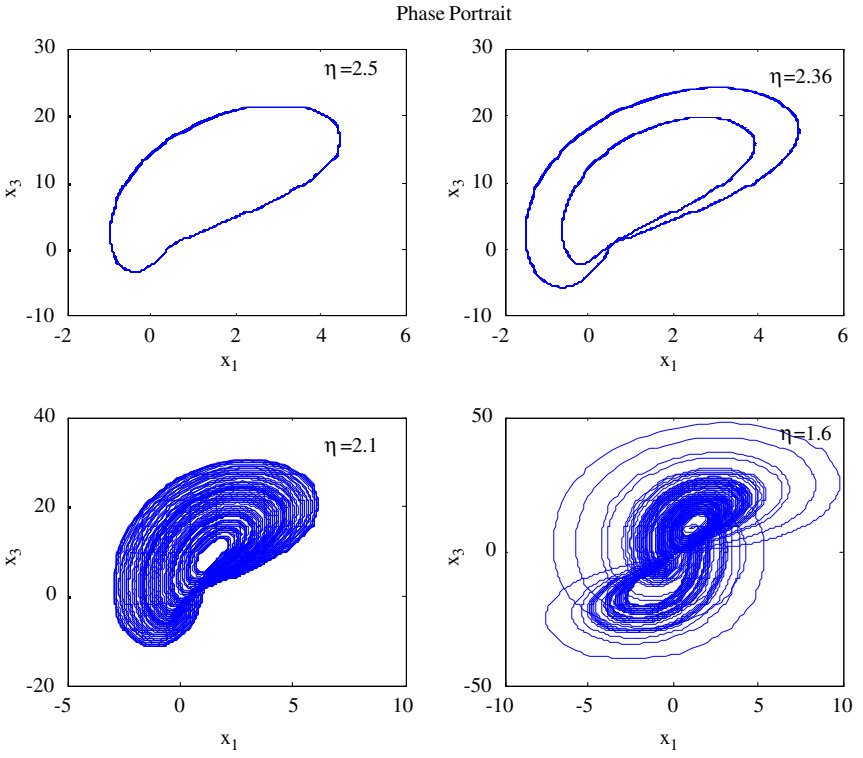

Fig. 2. Phase portrait with different η.

After transforming, the equations of motion are

$$\begin{aligned}\tau_1\frac{\mathrm{d}}{\mathrm{d}t} &= V_q - x_1 - x_2x_3 - x_3\\ \tau_2\frac{\mathrm{d}}{\mathrm{d}t} &= V_d + x_1x_3 - x_2\\ \tau_3\frac{\mathrm{d}}{\mathrm{d}t} &= \sigma x_1 + \rho x_1x_2 - \eta x_3 - \widetilde{T}_L\end{aligned} \tag{2.5}$$

where the nondimentional variables are

$$x_1 = \frac{L_q}{k_t\sqrt{\delta}}i_q,\quad x_2 = \frac{L_q}{k_t\delta}i_d,\quad x_3 = \frac{nL_q}{R\sqrt{\delta}}\omega,\quad V_q = \frac{L_q}{k_tR\sqrt{\delta}}v_q,\quad V_d = \frac{L_q}{k_tR\delta}v_d,$$

$$\sigma = n^2,\quad \rho = (1-\delta)n^2,\quad \eta = \frac{Rb}{k_t^2},\quad \tilde{t} = \frac{t}{t_3},\quad \widetilde{T}_L = \frac{nL_q}{k_t^2\sqrt{\delta}}T_L,\quad \delta = \frac{L_q}{L_d}$$

The period of autonomous system is hardly found, so we will modify the choice of Poincaré section for different inputs in Section 3. Almost the same bifurcation diagrams are obtained, because we only adjust a few positions of x_1 and x_3 axis from the original system. In addition, three time scales BLDCM is nondimensionalized. This means that all the inputs which we added are dimensionless. If we change them to the original system, all inputs have their physical meanings.

We will show the computational results such as phase portrait, bifurcation and Lyapunov exponents. Fig. 2 shows the phase portrait of various η. The motion is periodic for $\eta = 2.5$, 2.36, and for $\eta = 2.1$, 1.6 the motion is chaotic, and $\eta = 2.34$ is a critical value. Fig. 3 shows the bifurcation diagram and Lyapunov exponent. We observed that Lyapunov exponents $\lambda > 0$ where chaos presents in this figure.

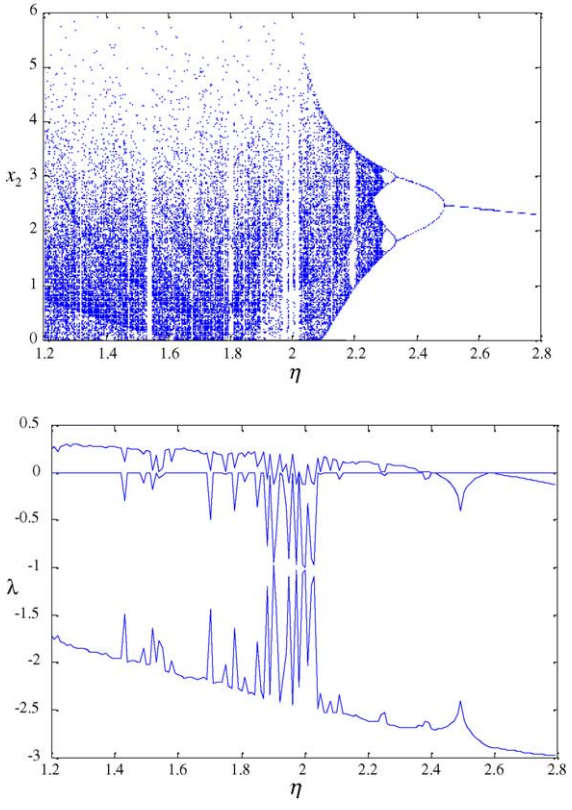

Fig. 3. Bifurcation diagram and Lyapunov exponents for three time scales system.

3. Anticontrol of chaos

In the following subsections, we will show the anticontrol by means of addition of a constant torque, a $x|x|$ term [12], and various periodic waves [11], such as the square wave, the triangle wave and the sawtooth wave.

3.1. Anticontrol of chaos by addition of a constant torque

One can add a constant torque U to anticontrol the regular dynamics to chaos dynamics in the following nonlinear autonomous system. The system is written as:

$$\begin{aligned}\tau_1\frac{\mathrm{d}}{\mathrm{d}t}x_1 &= V_q - x_1 - x_2x_3 - x_3\\ \tau_2\frac{\mathrm{d}}{\mathrm{d}t}x_2 &= V_d + x_1x_3 - x_2\\ \tau_3\frac{\mathrm{d}}{\mathrm{d}t}x_3 &= \sigma x_1 + \rho x_1x_2 - \eta x_3 - \widetilde{T_L} + U\end{aligned} \tag{3.1}$$

When $U = -2.0$, the bifurcation diagram is shown in Fig. 4. The corresponding Lyapunov exponent is plotted in Fig. 5. Comparing Figs. 3 and 4, the chaotic behavior increases.

3.2. Anticontrol of chaos by addition of a periodic term

3.2.1. Adding a periodic square wave

First, a periodic square wave input U is added. Consider U of period $2\pi/\omega$ is written as:

$$\begin{aligned}U &= \begin{cases} a, & \text{when } 0 \leqslant t < \pi/\omega \\ -a, & \text{when } \pi/\omega \leqslant t < 2\pi/\omega \end{cases}\\ &= -au(t) + 2a\sum_{k=0}^{\infty}\left[(-1)^k u\left(t - \frac{k\pi}{\omega}\right)\right]\end{aligned} \tag{3.2}$$

where a is the amplitude of square wave, ω the frequency of square wave, $u(t)$ the unit step function.

The system equations are

$$\begin{aligned}\tau_1\frac{\mathrm{d}}{\mathrm{d}t}x_1 &= V_q - x_1 - x_2x_3 - x_3\\ \tau_2\frac{\mathrm{d}}{\mathrm{d}t}x_2 &= V_d + x_1x_3 - x_2\\ \tau_3\frac{\mathrm{d}}{\mathrm{d}t}x_3 &= \sigma x_1 + \rho x_1x_2 - \eta x_3 - \widetilde{T}_L - au(t) + 2a\sum_{k=0}^{\infty}\left[(-1)^k u\left(t - \frac{k\pi}{\omega}\right)\right]\end{aligned} \tag{3.3}$$

For $\omega = 1$, and $a = 1$, the bifurcation diagram is shown in Fig. 6, and the corresponding Lyapunov exponent is shown in Fig. 7. Comparing with Fig. 3, the chaotic range has increased in some degree.

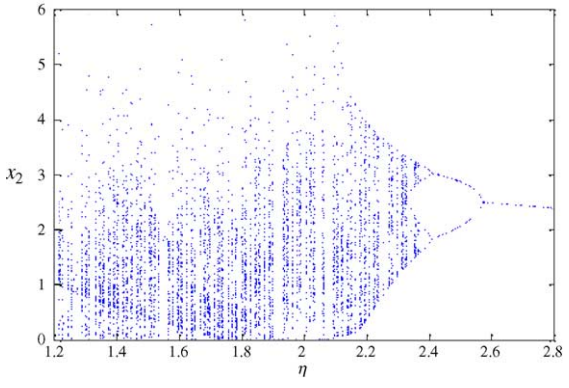

Fig. 4. Bifurcation diagram for constant torque $U = -2$.

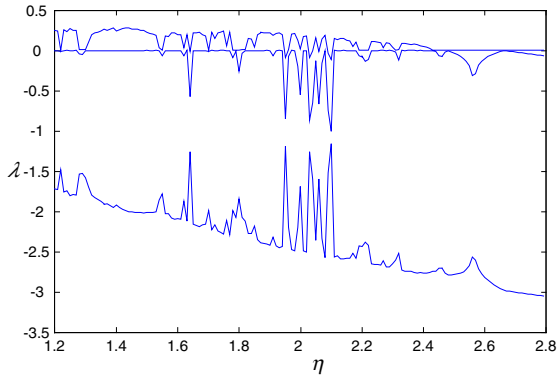

Fig. 5. Lyapunov exponents for constant torque $U = -2$.

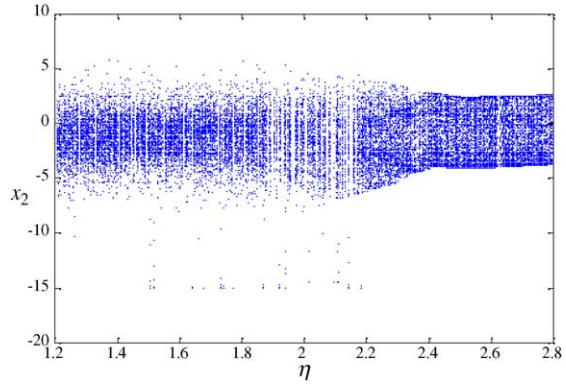

Fig. 6. Bifurcation diagram for periodic square wave U with $\omega = 1$, $a = 1$.

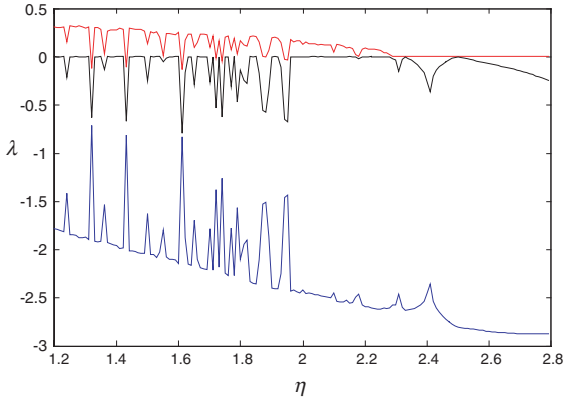

Fig. 7. Lyapunov exponents for periodic square wave U with $\omega = 1$, $a = 1$.

3.2.2. Adding a periodic saw tooth wave

In this section, a periodic sawtooth wave input U is added. Consider U of period $2\pi/\omega$ is written as:

$$\begin{aligned} U &= \frac{a\omega}{2\pi}t, \quad \text{when } 0 \leqslant t < 2\pi/\omega \\ &= \frac{a\omega t}{2\pi}u(t) - \sum_{k=0}^{\infty}\left[u\left(t - \frac{2(k+1)\pi}{\omega}\right)\right] \end{aligned} \tag{3.4}$$

where a is the amplitude of sawtooth wave, ω is the frequency of sawtooth wave, $u(t)$ is the unit step function.

The system equations are

$$\begin{aligned}
\tau_1 \frac{\mathrm{d}}{\mathrm{d}t} x_1 &= V_q - x_1 - x_2 x_3 - x_3 \\
\tau_2 \frac{\mathrm{d}}{\mathrm{d}t} x_2 &= V_d + x_1 x_3 - x_2 \\
\tau_3 \frac{\mathrm{d}}{\mathrm{d}t} x_3 &= \sigma x_1 + \rho x_1 x_2 - \eta x_3 - \widetilde{T}_L + \frac{a\omega t}{2\pi} u(t) - \sum_{k=0}^{\infty} \left[u\left(t - \frac{2(k+1)\pi}{\omega} \right) \right]
\end{aligned} \tag{3.5}$$

For $\omega = 1$, and $a = 1$, the bifurcation diagram is shown in Fig. 8, and the corresponding Lyapunov exponent is shown in Fig. 9. Comparing with Fig. 3, the chaotic range has increased in some degree.

3.2.3. Adding a periodic triangle wave

Finally, a periodic triangle wave input U is added. Consider U of period $2\pi/\omega$ is written as:

$$\begin{aligned}
U &= \begin{cases} \frac{a\omega}{\pi} t, & \text{when } 0 \leqslant t < \pi/\omega \\ a - \frac{a\omega}{\pi}\left(t - \frac{\pi}{\omega}\right), & \text{when } \quad \pi/\omega \leqslant t < 2\pi/\omega \end{cases} \\
&= -\frac{a\omega}{\pi} t u(t) + \sum_{k=0}^{\infty} \left[(-1)^k \left(\frac{2a\omega t}{\pi} - 2ka \right) u\left(t - \frac{k\pi}{\omega} \right) \right]
\end{aligned} \tag{3.6}$$

where a is the amplitude of triangle wave, ω is the frequency of square wave, $u(t)$ is the unit step function.

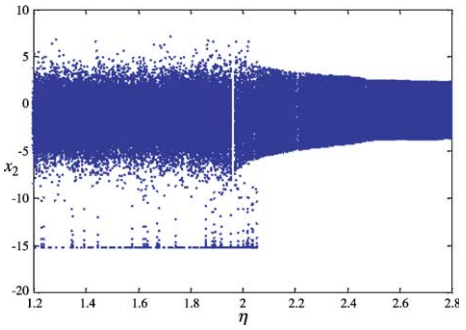

Fig. 8. Bifurcation diagram for periodic sawtooth wave U with $\omega = 1$, $a = 1$.

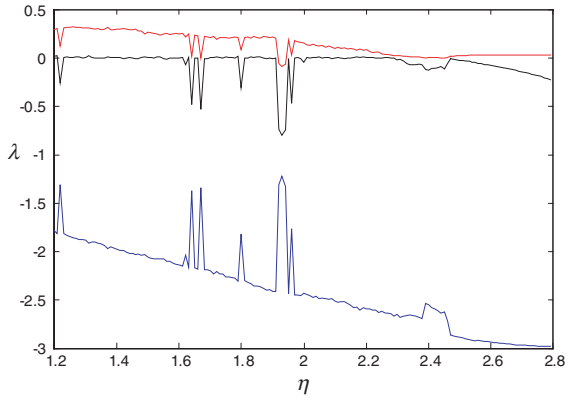

Fig. 9. Lyapunov exponents for periodic sawtooth square wave U with $\omega = 1$, $a = 1$.

The system equations are

$$\begin{aligned}
\tau_1 \frac{\mathrm{d}}{\mathrm{d}t} x_1 &= V_q - x_1 - x_2 x_3 - x_3 \\
\tau_2 \frac{\mathrm{d}}{\mathrm{d}t} x_2 &= V_d + x_1 x_3 - x_2 \\
\tau_3 \frac{\mathrm{d}}{\mathrm{d}t} x_3 &= \sigma x_1 + \rho x_1 x_2 - \eta x_3 - \widetilde{T}_L - \frac{a\omega}{\pi} t u(t) + \sum_{k=0}^{\infty} \left[(-1)^k \left(\frac{2a\omega t}{\pi} - 2ka \right) u\left(t - \frac{k\pi}{\omega} \right) \right]
\end{aligned} \tag{3.7}$$

For $\omega = 1$, and $a = 1$, the bifurcation diagram is shown in Fig. 10, and the corresponding Lyapunov exponent is shown in Fig. 11. Comparing with Fig. 3, the chaotic range has increased in some degree.

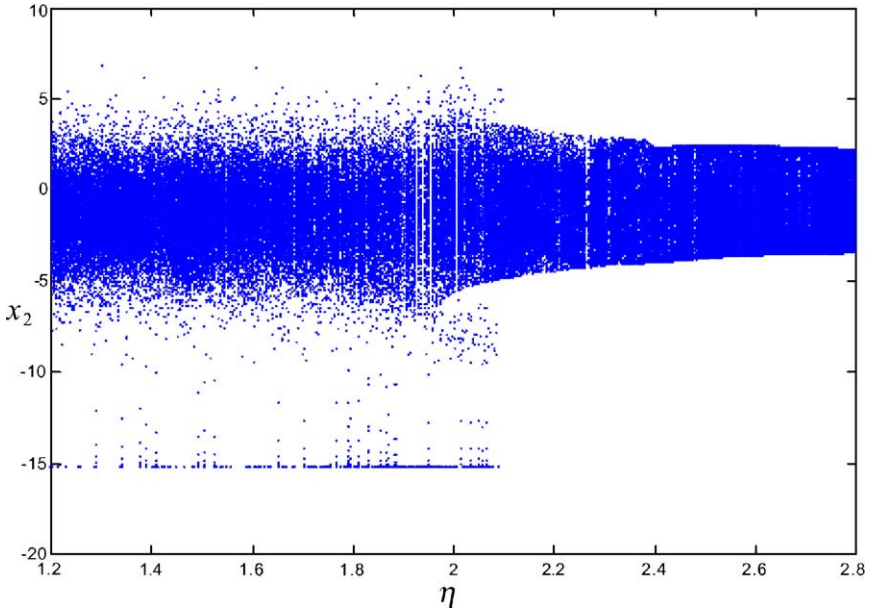

Fig. 10. Bifurcation diagram for periodic triangle wave U with $\omega = 1$, $a = 1$.

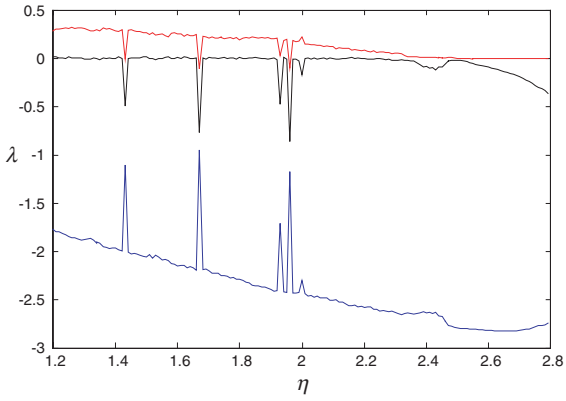

Fig. 11. Lyapunov exponents for periodic triangle wave U with $\omega = 1$, $a = 1$.

3.3. Anticontrol of chaos by addition of $kx|x|$

Similar to Section 3.2, $kx|x|$ can be added instead of periodic wave. We will apply it to each of system equations. Consider $U = k_1 x_1 |x_1|$, where k is the intensity constant. The equations can be written as:

$$\begin{aligned}
\tau_1 \frac{\mathrm{d}}{\mathrm{d}t} x_1 &= V_q - x_1 - x_2 x_3 - x_3 + k_1 x_1 |x_1| \\
\tau_2 \frac{\mathrm{d}}{\mathrm{d}t} x_2 &= V_d + x_1 x_3 - x_2 \\
\tau_3 \frac{\mathrm{d}}{\mathrm{d}t} x_3 &= \sigma x_1 + \rho x_1 x_2 - \eta x_3 - \widetilde{T}_L
\end{aligned} \tag{3.8}$$

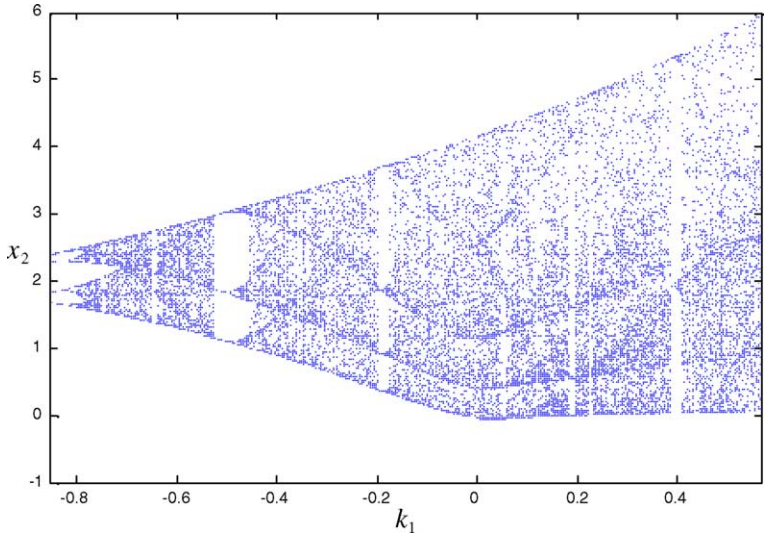

Fig. 12. Bifurcation diagram for $\eta = 2.1$, $k_1 = -0.85 \sim 0.5$.

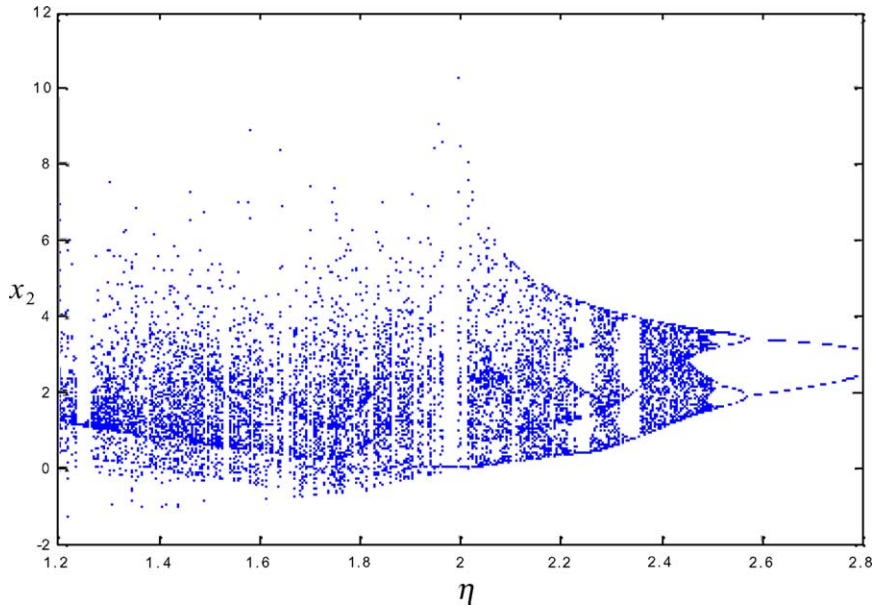

Fig. 13. Bifurcation diagram for $U = k_1 x_1 |x_1|$, $k_1 = 0.42$.

The physical meaning of U in the first equation is the external quadrature-axis voltage on the electric circuit. Without any inputs, when $\eta = 2.1$, the system is chaotic, and its bifurcation diagram versus k_1 is shown in Fig. 12. By choosing

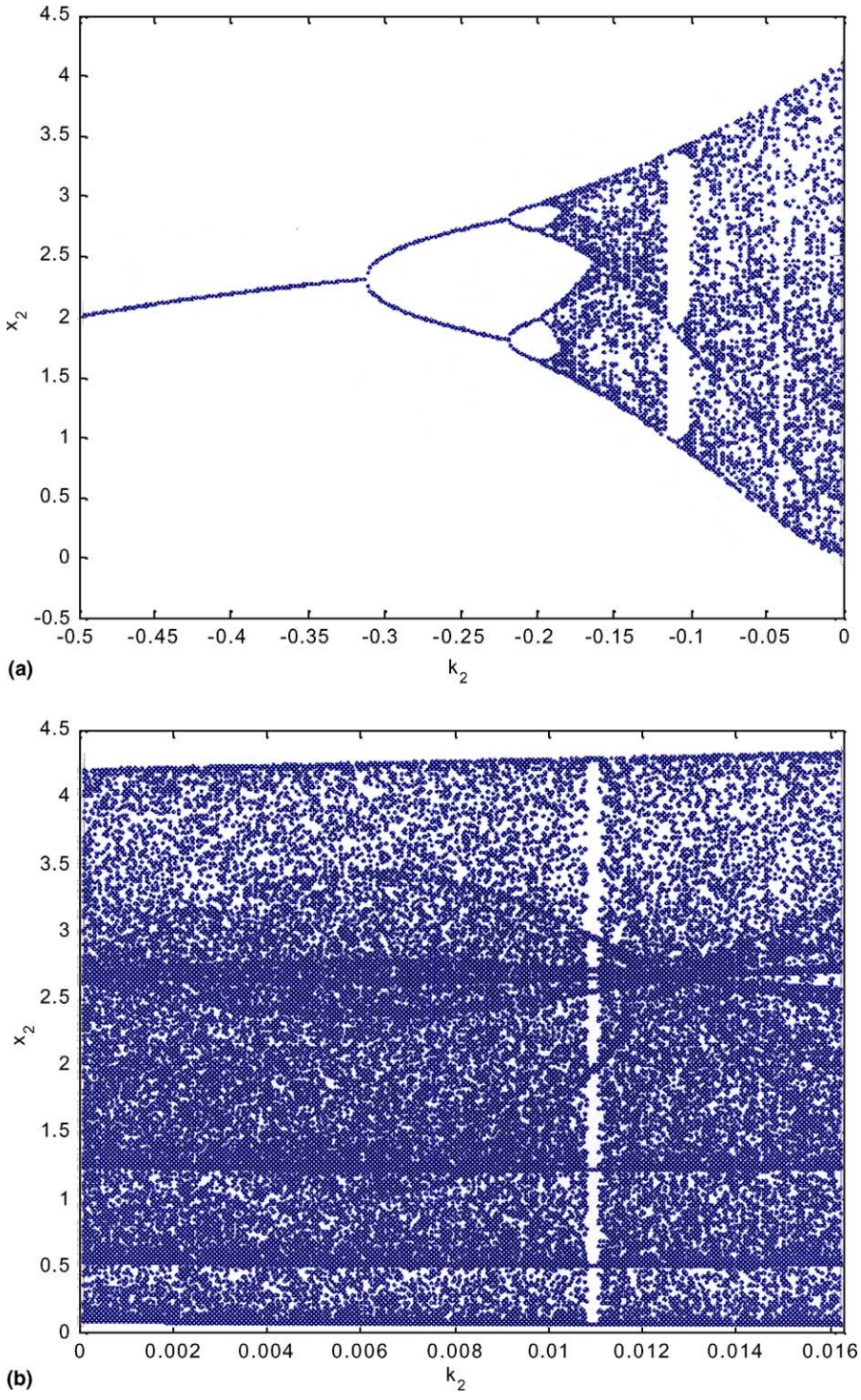

Fig. 14. Bifurcation diagram for $\eta = 2.1$: (a) $k_2 = -0.5 \sim 0$ and (b) $k_2 = 0 \sim 0.0163$.

$k_1 = 0.42$, the bifurcation diagram is plotted in Fig. 13. Comparing with the original system, the chaotic behavior has been increased effectively.

Next, we add $U = k_2 x_2 |x_2|$ in the second equation of the system. Here U means the external direct-axis voltage on the electrical circuit. Without any inputs, when $\eta = 2.1$, the system is chaotic, and its bifurcation diagram versus k_2 is shown in Fig. 14. By choosing $k_2 = -0.05$ and $k_2 = 0.014$, the bifurcation diagram is plotted in Fig. 15, and the corresponding Lyapunov exponent is shown in Fig. 16. Comparing with the original system, the chaotic behavior has increased in some degree.

Third, we add $U = k_3 x_3 |x_3|$ in the third equation of the system. Here U means the external torque on the rotator. Without any inputs, when $\eta = 2.1$, the system is chaotic, and its bifurcation diagram versus k_3 is shown in Fig. 17. By choosing $k_3 = 0.02$, the bifurcation diagram is plotted in Fig. 18, and the corresponding Lyapunov exponent is shown in Fig. 19. Comparing with the original system, the chaotic behavior has been increased effectively.

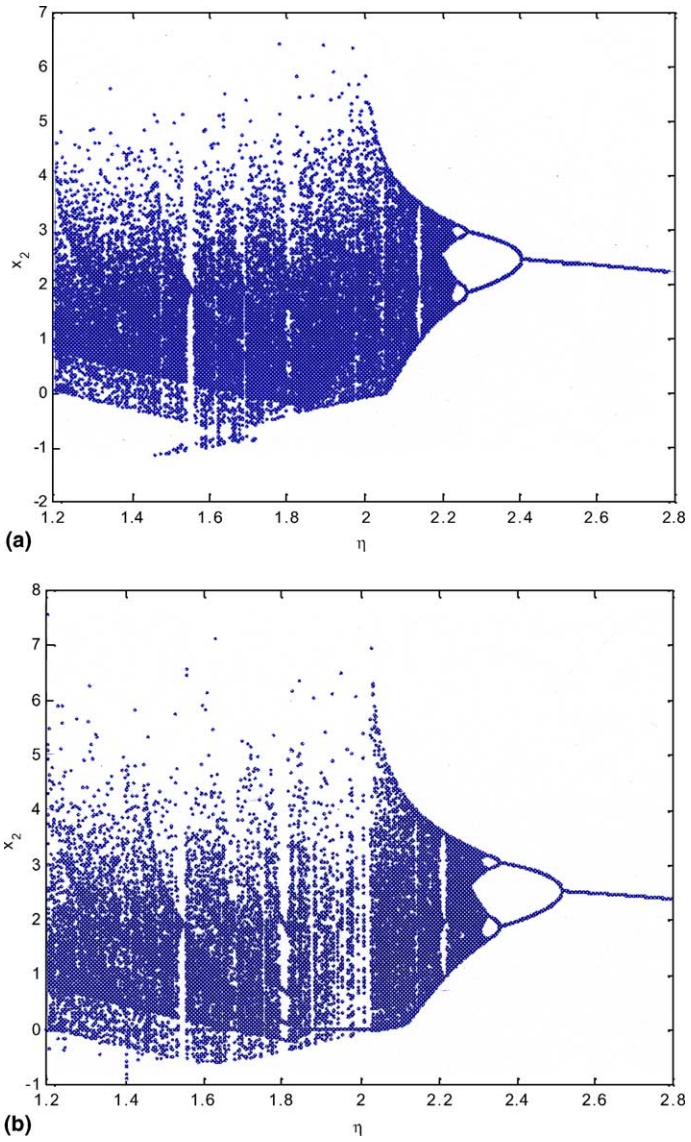

Fig. 15. Bifurcation diagram for $U = k_2 x_2 |x_2|$: (a) $k_2 = -0.05$ and (b) $k_2 = 0.014$.

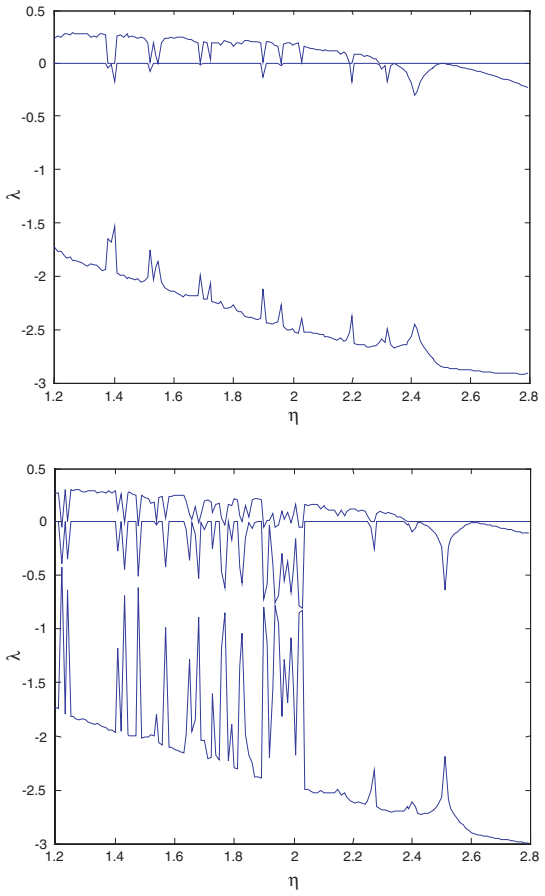

Fig. 16. Lyapunov exponents for $U = k_2 x_2 |x_2|$: (a) $k_2 = -0.05$ and (b) $k_2 = 0.014$.

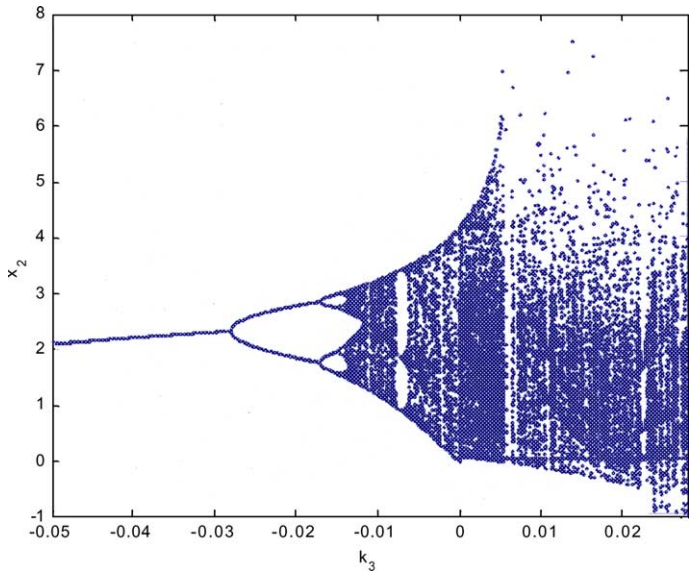

Fig. 17. Bifurcation diagram for $\eta = 2.1$, $k_3 = -0.05 \sim 0.028$.

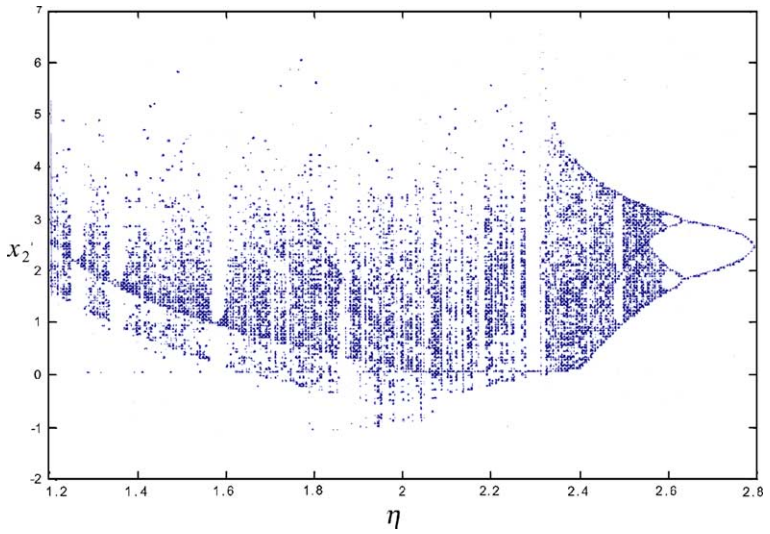

Fig. 18. Bifurcation diagram for $U = k_3 x_3 |x_3|$, $k_3 = 0.02$.

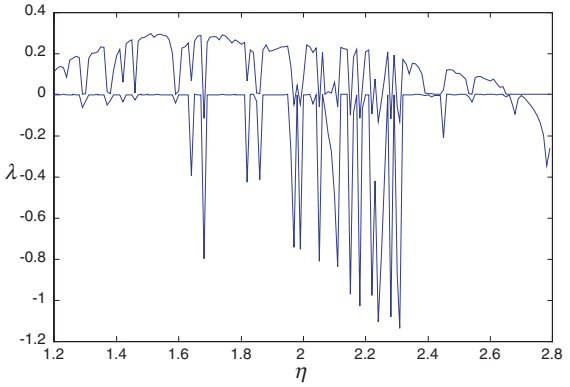

Fig. 19. Lyapunov exponents for $U = k_3 x_3 |x_3|$, $k_3 = 0.02$.

4. Chaos synchronization of different order systems

Third order BLDCM system and second order rate gyroscope system are used to achieve synchronization. The original three time scales BLDCM is the drive system

$$\begin{aligned}
\tau_1 \frac{\mathrm{d}}{\mathrm{d}t} x_1 &= V_q - x_1 - x_2 x_3 - x_3 \\
\tau_2 \frac{\mathrm{d}}{\mathrm{d}t} x_2 &= V_d + x_1 x_3 - x_2 \\
\tau_3 \frac{\mathrm{d}}{\mathrm{d}t} x_3 &= \sigma x_1 + \rho x_1 x_2 - \eta x_3 - \widetilde{T}_L
\end{aligned} \tag{2.5}$$

The response chaotic system, rate gyroscope, is written as [23]:

$$\begin{aligned}
\dot{y}_1 &= y_2 \\
\dot{y}_2 &= -2\alpha y_2 - y_1 - \beta \sin 2y_1 + \beta \sin 2y_1 \cos 2\omega t - \gamma \cos y_1 \sin \omega t
\end{aligned} \tag{4.1}$$

4.1. Synchronization of different order coupled chaotic systems

For the above systems, we choose x_3 to synchronize y_2. The coupling term $k(x_3 - y_2)$ is added to the response system, so the rate gyroscope system can be written as:

$$\begin{cases} \dot{y}_1 = y_2 \\ \dot{y}_2 = -2\alpha y_2 - y_1 - \beta \sin 2y_1 + \beta \sin 2y_1 \cos 2\omega t - \gamma \cos y_1 \sin \omega t + k(x_3 - y_2) \end{cases} \tag{4.2}$$

Fig. 20 shows $\int_{t_2}^{t_1} |e| \, dt/(t_2 - t_1) = \int_{t_1}^{t_2} |x_3 - y_2| \, dt/(t_2 - t_1)$ versus intensity k, where $|e|$ changes slowly in $t_1 - t_2$ interval. When $k = 10$, 100, and 1000, the time histories of errors are shown by Fig. 21(a)–(c). In Fig. 20, it is observed that $\int_{t_1}^{t_2} |e| \, dt/(t_2 - t_1) \approx 5.5$ around. Comparing (a)–(c) of Fig. 21, the larger the k, the smaller the ripple of errors, but more times spent to achieve generalized synchronization.

If we replace the drive and the response systems, that means we add the coupling term $k(y_2 - x_3)$ in BLDCM system, the result is shown in Figs. 22 and 23. Fig. 22 shows $\int_{t_1}^{t_2} |e| \, dt/(t_2 - t_1)$ versus k. It presents that the larger k gives the smaller ripples of error, and two different systems approach generalized synchronization.

4.2. Synchronization of different order systems by linearization of error dynamics

Similar to Section 4.1, we use the same systems to obtain synchronization. First, we add a state x_4 for original BLDCM system. We define $\tau_3 x_4$ as the angle of the motor, then we have the angular velocity

$$\omega = \frac{d(\tau_3 x_4)}{dt} = \tau_3 \frac{d}{dt} x_4 = x_3 \tag{4.3}$$

So the total three time scale BLDCM system can be written as:

$$\begin{aligned} \tau_1 \frac{d}{dt} x_1 &= V_q - x_1 - x_2 x_3 - x \\ \tau_2 \frac{d}{dt} x_2 &= V_d + x_1 x_3 - x \\ \tau_3 \frac{d}{dt} x_3 &= \sigma x_1 + \rho x_1 x_2 - \eta x_3 - \tilde{T}_L \\ \tau_3 \frac{d}{dt} x_4 &= x_3 \end{aligned} \tag{4.4}$$

which is a system with four state variables.

Then we add U in the rate gyroscope system to achieve synchronization by linearization [24]. Let

$$e = x_4 - y_1, \qquad \dot{e} = \dot{x}_4 - \dot{y}_1 = \tau_3 x_3 - y_2$$

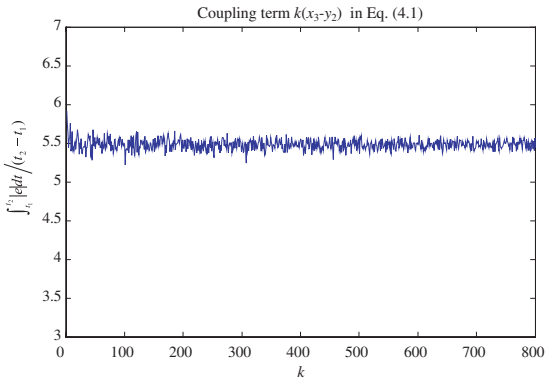

Fig. 20. $\int_{t_1}^{t_2} |e| \, dt/(t_2 - t_1)$ versus intensity k for different order synchronization of coupled term in $\dot{y}_2$.

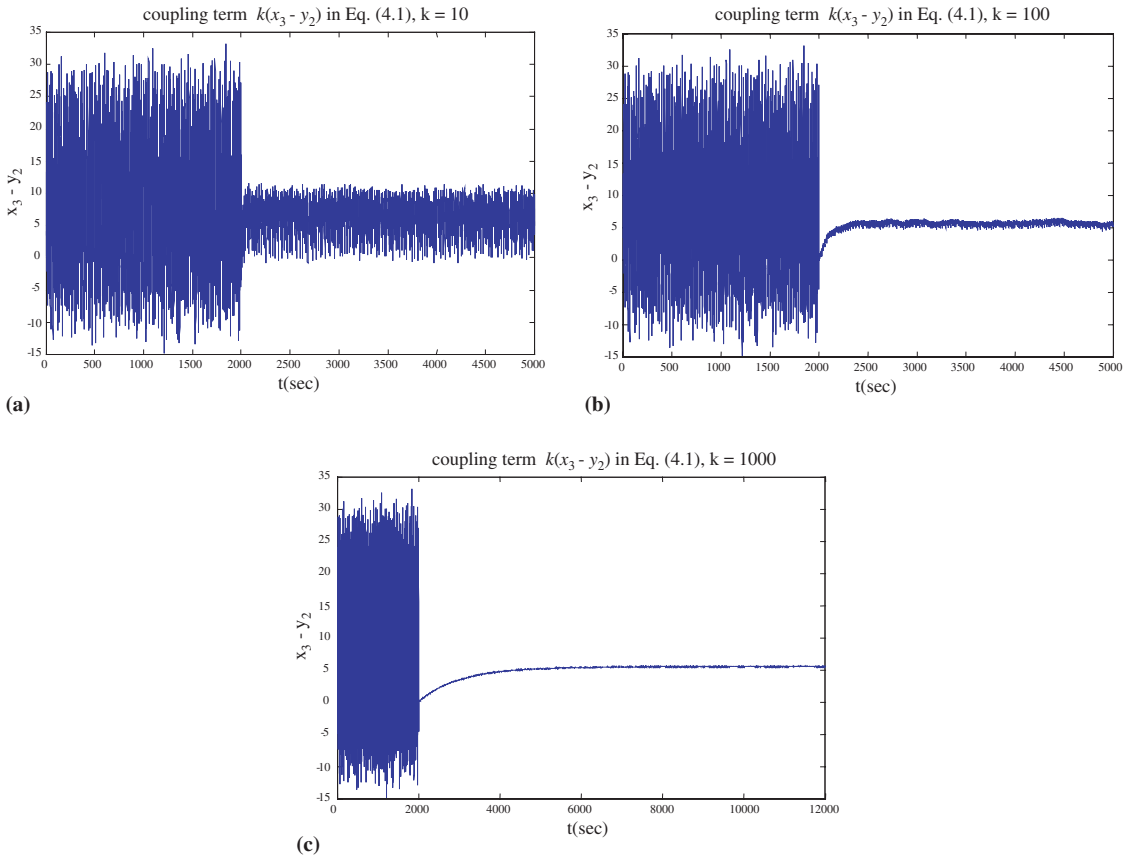

Fig. 21. Time histories of $x_3 - y_2$ of different order synchronization of coupled term in $\dot{y}_2$: (a) $k = 10$, (b) $k = 100$ and (c) $k = 1000$.

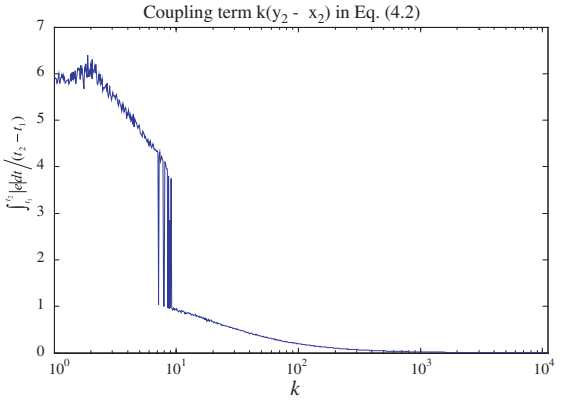

Fig. 22. $\int_{t_1}^{t_2} |e| \, \mathrm{d}t/(t_2 - t_1)$ versus intensity k for different order synchronization of coupled term $\dot{x}_3$.

$$\begin{aligned}\ddot{e} &= \tau_3(\sigma x_1 + \rho x_1 x_2 - \eta x_3 - T_L) + 2\alpha y_2 + y_1 + \beta \sin 2y_1 - \beta \sin 2y_1 \cos 2\omega t + r \cos x_1 \sin \omega t + U \\ &= -e - \eta \dot{e} + [(2\alpha - \eta) y x_1 x_2 + x_4 + \tau_3 \rho x_1 x_2 - \tau_3 \widetilde{T}_L + \beta \sin 2y_1 - \beta \sin 2y_1 \cos 2\omega t + \gamma \cos x_1 \sin \omega t] - U \\ &= -e - \eta \dot{e} + \tau_e'(x, y, t) - U\end{aligned}$$

where

$$\tau_e'(x,y,t) = (2\alpha-\eta)yx_1x_2 + x_4 + \tau_3\rho x_1x_2 - \tau_3\widetilde{T}_L + \beta\sin 2y_1 - \beta\sin 2y_1\cos 2\omega t + \gamma\cos x_1\sin\omega$$

Let

$$e_1 = e = x_4 - y_1, \qquad e_2 = \dot{e} = \tau_3 x_3 - y_2$$

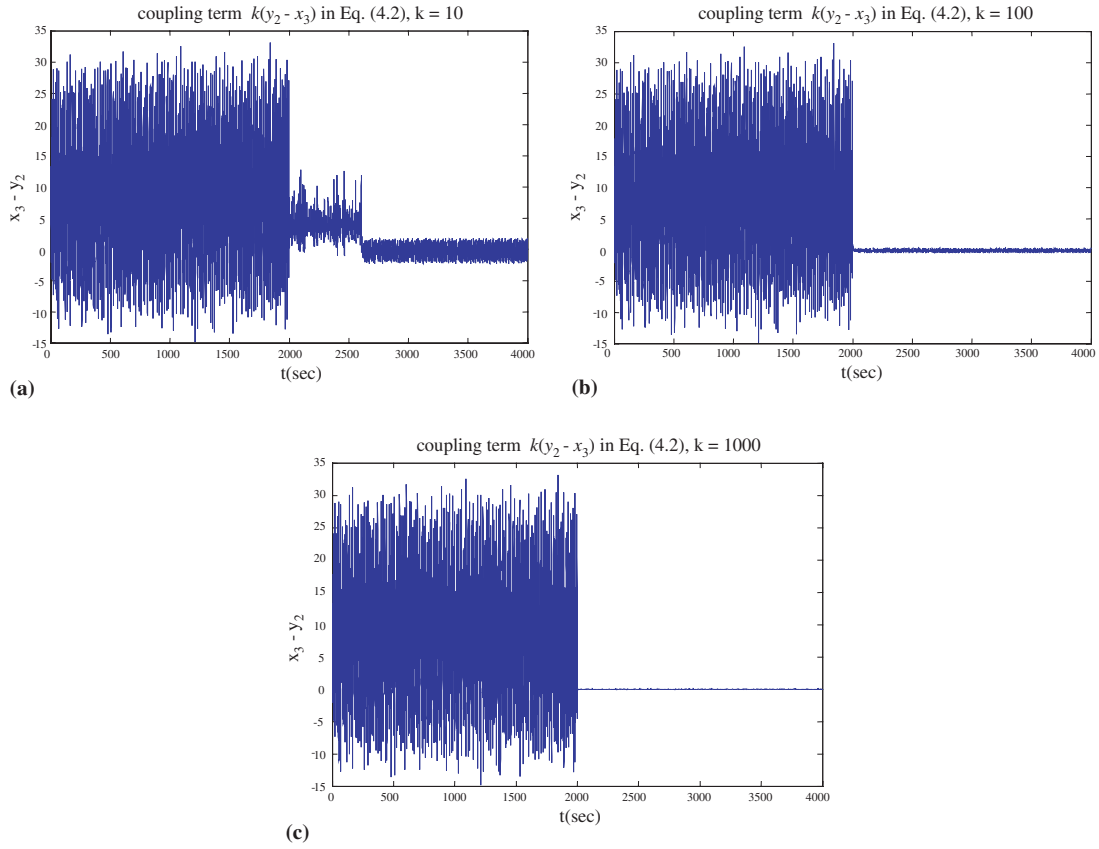

Fig. 23. Time histories of $x_3 - y_2$ of different order synchronization of coupled term in $\dot{x}_3$: (a) $k = 10$, (b) $k = 100$ and (c) $k = 1000$.

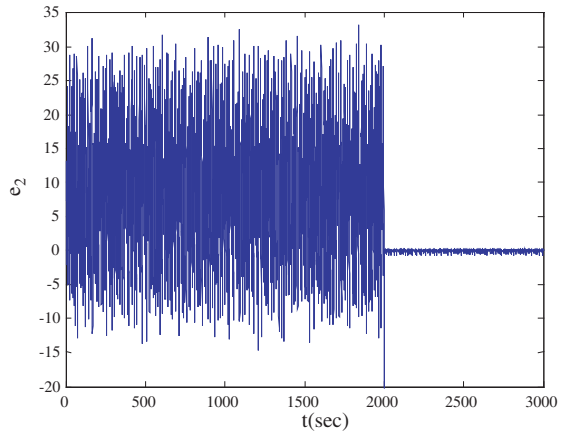

Fig. 24. Time histories of e_2 after linearization different order synchronization.

$$\begin{cases} \dot{e}_1 = e_2 \\ \dot{e}_2 = -e_1 - \eta e_2 + \tau_e'(x,y,t) - U \end{cases} \tag{4.5}$$

And let $U = \tau_e'(x,y,t) + k_1 e_1 + k_2 e_2$, Eq. (4.5) can be written as

$$\dot{e} = \begin{bmatrix} \dot{e}_1 \\ \dot{e}_2 \end{bmatrix} = \begin{bmatrix} 0 & 1 \\ -1-k_1 & -\eta - k_2 \end{bmatrix} \begin{bmatrix} e_1 \\ e_2 \end{bmatrix} = Ae$$

If the all eigenvalues of A are less than 0, $e(t)$ converges to zero. We take both eigenvalues of A as 20, −20, we get $k_1 = 399$, $k_2 = 57.9$, and $U(t) = \tau_e'(x,y,t) + 399e_1 + 57.9e_2$.

Fig. 24 shows e_2 versus the time. The system can be partially synchronized with a small error, i.e. the systems are practically synchronized.

5. Conclusions

First, we present the blushless dc motor (BLDCM) system that is transformed to a nondimensionalized form. Then we study the behavior of BLDCM via numerical simulation. After applying the numerical results such as phase portrait, and bifurcation, a variety of the phenomena of the chaotic motion can be presented. Furthermore, Lyapunov exponents can also be used to check the chaotic motion. Anticontrol of chaos is studied via adding a constant torque, a $x|x|$ term, and various periodic waves, such as the square wave, the triangle wave, and the sawtooth wave. Finally, the chaos synchronization of two different order systems, i.e. the BLDCM system and rate gyroscope system, can be achieved via various coupling terms, and linearization of error dynamics.

Acknowledgements

This research was supported by the National Science Council, Republic of China, under Grant Number NSC 92-2212-E-009-027.

References

[1] Schiff SJ, Jerger K, Duong DH, Chang T, Spano ML, Ditto WL. Controlling chaos in the brain. Nature 1994;370:615–20.
[2] Ott E. Chaos in dynamic systems. second ed. England: Cambridge; 2002.
[3] Chen G, Dong X. From chaos to order. New Jersey: World Scientific; 1998.
[4] Nemati H. Dynamic analysis of brushless motors based on compact representations of the equations of motion. IEEE Indus Appl Soci Annu Meeting 1993;1:51–8.
[5] Nemati H. Strange attractors in brushless DC motors. IEEE Trans Circ Syst 1994;41(1):40–5.
[6] Chen G. Control and anticontrol of chaos. In: Proceedings of the 1st International Conference on Oscillations and Chaos, St. Petersburg, Russia, 1997. p. 181–6.
[7] Wang X-F, Chen G, Man KF. Chaotifying a continuous-time system by time-delay feedback. In: IEEE International Symposium on Circuits and Systems, 2000. p. II116–9.
[8] Chen G, Lai D. Anticontrol of chaos via feedback. In: Proceedings of the 36th Conference on Decision and Control, 1997. p. 367–72.
[9] Wang X-F, Chen G. Chaotification via arbitrarily small feedback controls: Theory, method, and applications. Int J Bifurcat Chaos 2000;10:549–70.
[10] Wang X-F, Chen G. Chaotifying a stable LTI system by tiny feedback control. IEEE Trans Circ Syst I 2000;47:410–5.
[11] Wang X-F, Chen G Man, Man KF. Chaotifying a stable LTI system by tiny feedback control. IEEE Trans Circ Syst I 2001;48:641–5.
[12] Tang K-S, Man KF, Zhong G-Q, Chen G. Generating chaos via $x|x|$. IEEE Trans Circ Syst I 2001;48:636–41.
[13] Wang X-F et al. Generating chaos in chua's circuit via time-delay feedback. IEEE Trans Circ Syst I 2001;48:1151–6.
[14] Li Z, Park JB, Joo YH. Chaotifying continuous-Time TS Fuzzy via Discretization. IEEE Trans Circ Syst I 2001;48:1237–43.
[15] Sanchez EN, Perez JP, Chen G. Using dynamical neural networks to generate chaos: An inverse optimal control approach. Int J Bifurcat Chaos 2001;11:857–63.
[16] Zhong G-Q, Man KF, Chen G. Generating chaos via dynamical controller. Int J Bifurcat Chaos 2001;11:865–9.
[17] Lu H, Tang WKS. Chaotic phase shift keying in delayed chaotic anticontrol systems. Int J Bifurcat Chaos 2002;12:1017–28.
[18] Li Z et al. Anticontrol of chaos for discrete TS fuzzy systems. IEEE Trans Circ Syst I 2002;49:249–53.
[19] Bondarenko VE. Control and 'anticontrol' of chaos in an analog neural network with time delay. Chaos, Solitons & Fractals 2002;13:139–54.

[20] Codreanu S. Desynchronization and chaotification of nonlinear dynamical systems. Chaos, Solitons & Fractals 2002;13:839–43.
[21] Wang X-F, Chen G. Generating topological conjugate chaotic systems via feedback control. IEEE Trans Circ Syst I 2003;50:812–7.
[22] Chen H-K, Lee C-I. Anti-control of chaos in rigid body motion. Chaos, Solitons & Fractals 2004;21:957–65.
[23] Ge Z-M, Chen H-H. Bifurcations and chaotic motions in a rate gyro with sinusoidal velocity about spin axis. J Sound Vib 1997;200(2).
[24] Pecora LM, Carroll TL. Synchronization in chaotic systems. Phys Rev Lett 1990;64:821–4.
[25] Ruan J, Li L. An improved method in synchronization of chaotic systems. Commun Nonlinear Sci Numer Simulat 1998;3:140–3.
[26] Huang Z, Ruan J. Synchronization of chaotic systems by linear feedback controller. Commun Nonlinear Sci Numer Simulat 1998;3:27–30.
[27] Zeng X, Ruan J, Li L. Synchronization of chaotic systems by feedback. Commun Nonlinear Sci Numer Simulat 1999;4:162–5.
[28] Wang C, Ge SS. Adaptive synchronization of uncertain chaotic systems via backstepping design. Chaos, Solitons & Fractals 2001;12:1026–199.
[29] Hegazi AS, Agiza HN, EI Dessoky MM. Synchronization and adaptive synchronization of nuclear spin generator systems. Chaos, Solitons & Fractals 2001;12:1091–9.
[30] Chen S, Lü J. Synchronization of an uncertain chaotic system via adaptive control. Chaos, Solitons & Fractals 2002;14:643–7.
[31] Liu F et al. A linear feedback synchronization theorem for a class of chaotic systems. Chaos, Solitons & Fractals 2002;13:723–30.
[32] Tan X, Zhang J, Yang Y. Synchronizing chaotic systems using backsteping design. Chaos, Solitons & Fractals 2003;16:37–45.
[33] Codreanu S. Synchronization of spatiotemporal nonlinear dynamical systems by an active control. Chaos, Solitons & Fractals 2003;15:507–10.
[34] Chen M, Han Z. Controlling and synchronizing chaotic genesio system via nonlinear feedback control. Chaos, Solitons & Fractals 2003;17:709–16.
[35] Lu J, Xi Y. Linear generalized synchronization of continuous-time chaotic systems. Chaos, Solitons & Fractals 2003;17:825–31.
[36] Femat R, Gualberto S-P. Synchronization of chaotic system with different order. Phys Rev E 2002;65:036226-1–7.
[37] Sun J, Zhang Y. Some simple global synchronization criterions for coupled time-varying chaotic systems. Chaos, Solitons & Fractals 2004;19:93–8.